LETTER

Experimental determination of the bulk Rashba parameters in BiTeBr

To cite this article: C. Martin *et al* 2016 *EPL* **116** 57003

A Letters Journal Exploring the Frontiers of Physics

December 2016

EPL, **116** (2016) 57003 www.epljournal.org
doi: 10.1209/0295-5075/116/57003

Experimental determination of the bulk Rashba parameters in BiTeBr

C. Martin[1], A. V. Suslov[2], S. Buvaev[3], A. F. Hebard[3], P. Bugnon[4], H. Berger[4], A. Magrez[4] and D. B. Tanner[3]

[1] *Ramapo College of New Jersey - Mahwah, NJ, 07430, USA*
[2] *National High Magnetic Field Laboratory - Tallahassee, FL, 32310, USA*
[3] *Department of Physics, University of Florida - Gainesville, FL, 32611, USA*
[4] *Crystal Growth Facility, Ecole Polytechnqiue Federale de Lausanne - CH-1015 Lausanne, Switzerland*

received 19 October 2016; accepted in final form 4 January 2017
published online 20 January 2017

PACS 78.40.Fy – Semiconductors
PACS 78.30.-j – Infrared and Raman spectra
PACS 78.20.-e – Optical properties of bulk materials and thin films

Abstract – Shubnikov-de Haas (SdH) oscillations, Hall effect, and optical reflectance ($\mathcal{R}(\omega)$) measurements have been performed on single crystals of BiTeBr. Under magnetic fields up to 32 tesla and at temperatures as low as 0.4 K, the SdH data shows a single oscillation frequency $F = 102 \pm 5$ tesla. The combined transport and optical studies establish that the SdH effect originates from the Rashba spin-split bulk conduction band, with the chemical potential situated about 13 meV below the crossing (Dirac) point. The bulk carrier concentration was $n_e \approx 5 \times 10^{18}\,\mathrm{cm}^{-3}$ and the effective mass $m_1^* = 0.16m_0$. Combining SdH and optical data, we reliably determine the Rashba parameters for the bulk conduction band of BiTeBr: the Rashba energy $E_R = 28$ meV and the momentum spin-split $k_R = 0.033\,\text{Å}^{-1}$. Hence, the bulk Rashba coupling strength $\alpha_R = 2E_R/k_R$ is found to be 1.7 eVÅ.

Introduction. – Manipulating the spin of electrons for technological applications (high-speed electronics, high volume storage, quantum computing), or for the realization of spin-related phenomena (spin Hall effect, triplet superconductivity, Majorana fermions) relies on lifting the degeneracy between the up and down projections of the electron spin, imposed in electronic materials by the combination of time-reversal symmetry and inversion symmetry. In general, this can be realized by an applied magnetic field $\mathbf{H}$, *i.e.*, Zeeman effect, which breaks the time-reversal symmetry by coupling $\mathbf{H}$ and the spin $\boldsymbol{\sigma}$. In recent years, however, there has been a remarkable interest in using the spin-orbit coupling (SOC) as an alternative mechanism. SOC lifts the spin degeneracy by coupling the motion of the electron, *i.e.*, momentum $\mathbf{k}$ and its spin $\boldsymbol{\sigma}$, through an effective spin-orbit magnetic field $\mathbf{H}_{SO} \propto \boldsymbol{k} \times \boldsymbol{\sigma}$. What is exciting about this mechanism is that it allows for spin manipulation without the complications of an applied external magnetic field, and rather by electrical means, opening the doors for a new branch of spintronics without externally applied magnetic field [1].

The V-VI-VII layered semiconductors BiTeX (X = Cl, Br, I) have emerged as very promising SOC materials. The inversion-asymmetric crystal structure and the large spin-orbit interaction originating from Bi give rise to a large shift of their electronic bands in momentum space, *i.e.*, Rashba spin-splitting. The Rashba effect plays a very important role in the field of spin-related devices and phenomena, and, therefore, continues to represent a hot topic in condensed-matter physics [2]. The magnitude of the effect is quantified in terms of the Rashba coupling parameter $\alpha_R = 2E_R/k_R$, which connects the splitting energy E_R and the splitting momentum k_R [3]. A large coupling parameter is needed for applications. In engineered interfaces or surfaces, α_R is typically smaller than 1 eVÅ, but there are reports of values up to 3 eVÅ for Bi atoms on the surface of Cu or Ag alloys [4,5].

In contrast, angular resolved photoemission spectroscopy (ARPES) measurements and band structure calculations show that BiTeI has a Rashba coupling parameter as high as $\alpha_R \approx 4$–5 eVÅ [6], and unlike in two-dimensional structures, the spin splitting occurs within the

bulk electronic bands. BiTeI consists of ionically bound Bi, Te and I three-layers, with the three-layers stacked by van der Waals interactions. This gives rise to a crystal structure without inversion symmetry (the P3m1 space group symmetry), which together with spin-orbit interaction is at the center of spin splitting. Theoretical work has shown that, additionally, BiTeI fulfills other requirements for a bulk character of the splitting, such as narrow band gap and identical symmetries of the top valence and bottom conduction bands [7].

Subsequently, this bulk Rashba effect has been both observed and calculated in the similar compounds BiTeCl and BiTeBr. The existence of surface states has also been demonstrated in these materials [6,8,9]. Furthermore, it was shown that BiTeI becomes a topological insulator under pressure [10–12], while BiTeCl has topologically protected surface states even at ambient pressure [13] and it becomes a superconductor under pressure, possibly the first example of a topological superconductor [14]. There are, however, unsettled questions regarding both the bulk and the surface properties. For BiTeBr in particular, the reported values of the bulk Rashba parameter differ by almost a factor of two, from about 2 eVÅ for theoretical calculations [15,16] to 4 eVÅ for ARPES results [17]. In this letter, we show that by combining Shubnikov-de Haas oscillations and infrared optical reflectance, we can determine reliably the momentum and energy splitting, and hence the value of the Rashba parameter α_R for the bulk conduction band of BiTeBr.

Experimental. – We studied single crystals with approximate dimensions $5 \times 3 \times 0.1\,\mathrm{mm}^3$, selected from a batch grown and characterized according to ref. [18]. Shubnikov-de Haas measurements were performed in Cell 9 at the National High Magnetic Field Laboratory. This facility combines a top loading ^{3}He cryostat, with sample in liquid, and a 32 tesla resistive magnet. Additional measurements of temperature-dependent resistance and Hall effect were performed using a commercial PPMS system from Quantum Design. Room temperature optical reflectance data ($\mathcal{R}(\omega)$), at frequencies between $30\,\mathrm{cm}^{-1}$ and $32000\,\mathrm{cm}^{-1}$ (4 meV–4 eV), were taken using a combination of a Bruker 113v Fourier spectrometer and a Zeiss microscope photometer. Then, Kramers-Kronig analysis was used to estimate the optical conductivity $\sigma_1(\omega)$, using an extrapolation procedure described in ref. [19]. On cleaving a thin layer from a crystal, we found that the sample also transmits below the band gap and above the free-carrier band; we measured transmittance at temperatures between 30 and 300 K.

Results and discussion. – The lower inset of fig. 1 shows the temperature dependence of the resistance, $R(T)$. It can be seen that the resistance has a metallic character, decreasing by a factor of about two upon cooling from room temperature to 5 K. This behavior is consistent with most Bi-based semiconductors whose chemical potential lies above the conduction band minimum. A small upturn of $R(T)$ is observed below 20 K; its cause remains to be further investigated. From Hall measurements we found that the carriers are electrons with a concentration $n \approx 5 \times 10^{18}\,\mathrm{cm}^{-3}$, constant with temperature. The main panel of fig. 1 shows the magnetic-field dependence of the Hall resistance at $T = 0.4$ K, in magnetic field up to 32 tesla. The SdH oscillations are clearly visible above 15 tesla. After subtracting the smooth background and performing a Fourier transform of $R_{Hall}(1/B)$, we found a single frequency $F = 102 \pm 5$ T. While it does not prove the Rashba effect in BiTeBr, the existence of only one SdH oscillation may still consistent with a spin-split conduction band, when the Fermi energy is situated below the crossing (Dirac) point, as sketched in the upper inset of fig. 1. In this case the spectrum has only one frequency, corresponding to the outer extreme orbit. We calculated the corresponding momentum $k_{out} = 0.056 \pm 0.001\,\text{Å}^{-1}$.

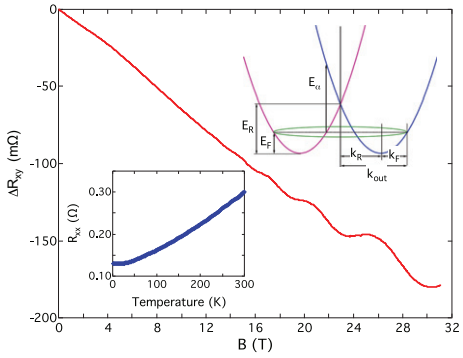

Fig. 1: (Color online) Main panel: Hall resistance *vs.* magnetic field of BiTeBr at $T = 0.4$ K, showing SdH oscillations at higher fields. Lower inset: R_{xx} *vs.* T of BiTeBr. Upper inset: sketch of a Rashba spin-split conduction band; different colors suggest opposite in-plane component of the electron spin. The outer extreme electronic orbit with momentum k_{out} gives rise to the SdH oscillations in the main panel. E_R and k_R represent the Rashba energy and momentum, respectively. E_F and k_F are the Fermi energy, measured from the bottom of the conduction band and the Fermi momentum, respectively. E_α is the onset of the direct intraband transition between branches with opposite spins.

The main panel of fig. 2 shows the evolution with temperature between 0.4 and 35 K of SdH oscillations in the resistance. A relatively slow suppression of amplitude with increasing temperature can be observed, specific to a low effective mass. In the inset of fig. 2 we plot the temperature dependence of the amplitude of the oscillation at $1/B = 0.0385\,\mathrm{T}^{-1}$, or $B = 26$ T. A fit to the Lifshitz-Kosevich formula [20] yields an effective mass $m^* = (0.15 \pm 0.01)m_0$, where m_0 is the free-electron mass. This value is very similar to previous findings for BiTeI and BiTeCl [21,22].

The existence of surface states in BiTeBr has been established both theoretically and from ARPES data, and it is still debated whether they form a quantum well due to surface bending of the conduction band or instead a distinct two-dimensional conducting layer that separates

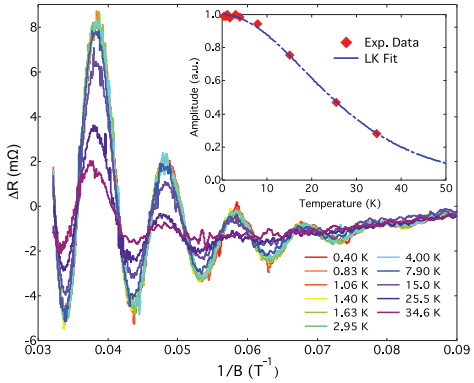

Fig. 2: (Color online) ΔR *vs.* $1/B$ (with B applied perpendicular to the sample surface) at temperatures from 0.4 to 40 K Inset: amplitude of the SdH oscillations at $B = 0.0385\,\mathrm{T}^{-1}$ (red symbols) and a fit (blue line) to the temperature dependence of the Lifshitz-Kosevich formula [20].

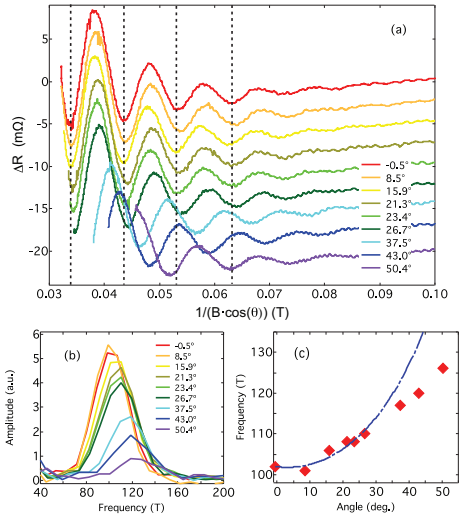

Fig. 3: (Color online) (a) $\Delta R(1/B)$ at different angles between the magnetic field and sample surface, plotted against the field component along the normal to the sample surface. The dashed lines indicate the positions of minima when the field is normal to the sample surface. (b) Fourier transform of the data from the main panel. (c) Amplitude of the oscillation at $B = 0.0385\,\mathrm{T}^{-1}$ (red symbols) and a fit (blue line) to the angle dependence $1/\cos(\theta)$.

from the bulk [15–17]. It is therefore imperative to establish the origin of the SdH effect observed in our data: surface or bulk? We will make the case that our results strongly support SdH oscillations of bulk carriers; moreover, we provide, to the best of our knowledge, the first reliable experimental characterization of the bulk electronic properties of BiTeBr.

First, we look in fig. 3(a) at the angle dependence of the SdH oscillations (at $T = 0.4\,\mathrm{K}$), displayed as a function of the magnetic-field component perpendicular to the sample surface ($B\cos(\theta)$). At angles above $\theta \approx 30°$, it appears obvious that the oscillations no longer scale with the normal component of the magnetic field. Also, if we plot either the position of the peak from the Fourier transform, shown in fig. 3(b) or the location of a particular minimum in the oscillations, we can see in fig. 3(c) that at higher angles there is clear departure from the $1/\cos(\theta)$ behavior expected for a two-dimensional Fermi surface. This strong evidence for a three-dimensional Fermi surface basically rules out possible surface origin of the SdH oscillations. SdH oscillations of carriers confined to a surface should have a strong two-dimensional character and should have scaled well with the normal component of the field. Moreover, a strong suppression of the amplitude with tilting magnetic field is expected for surface oscillations; the oscillations in fig. 3 remain prominent up to an angle as high as 50°.

Second, we compare the results from Hall effect and SdH oscillations with those from infrared optical reflectance $\mathcal{R}(\omega)$, shown in fig. 4(a). We showed previously [21] for the case of BiTeI that a monolayer-thick conducting surface layer, with impedance $R_\square \sim 2000\,\Omega_\square$, affects the far-infrared reflectance of a conductor with conductivity of order $\sigma_1 \sim 100\,\Omega^{-1}\,\mathrm{cm}^{-1}$ by less than 0.5%. Therefore, $\mathcal{R}(\omega)$ of BiTeBr, shown in fig. 4(a), should be governed almost entirely by the response of the bulk. The low-frequency reflectance is about 90%. A plasma edge can be clearly observed in the midinfrared spectral range, supporting the metallic nature of the bulk of BiTeBr. Sharp phonon modes are also observed at low frequencies. These phonon modes will be discussed elsewhere.

The optical conductivity, $\sigma_1(\omega)$, (from Kramers-Kronig analysis) is shown in the inset of fig. 4(a). A strong absorption edge, associated with the semiconducting gap E_g and several interband transitions dominate the midinfrared range. The optical conductivity rises rapidly above 0.5 eV, suggesting a gap near this value. The more accurate estimate of the band gap is obtained from measurements of transmittance, shown at 30 and 300 K in the inset of fig. 4(b). As can be observed, there is transmission at energies between 250 meV and 600 meV. The higher-frequency cut-off (edge) at 600 meV is associated with the onset of direct interband transitions between the valence and the conduction bands, *i.e.*, across the band gap. A 40 meV shift with temperature can be clearly seen. Now, the estimate of E_g also depends on the position of the chemical potential. However, we will show later that the electron concentration in the present sample puts the Fermi level only about 13 meV above the conduction band minimum, making our estimate of $E_g \approx 600$ meV a valid one. This value is in very good agreement with a previous optical study [23] and shows that the band gap in BiTeBr is almost twice as large as in BiTeI, thus making BiTeBr appealing for practical applications.

The low-frequency optical conductivity contains a clear zero-frequency (Drude) peak and sharp phonon modes. The dc conductivity is $\sigma(0) \approx 200\,\Omega^{-1}\mathrm{cm}^{-1}$, *i.e.*, $\rho_0 \approx 5\,\mathrm{m}\Omega\cdot\mathrm{cm}$, characteristic of a moderately doped

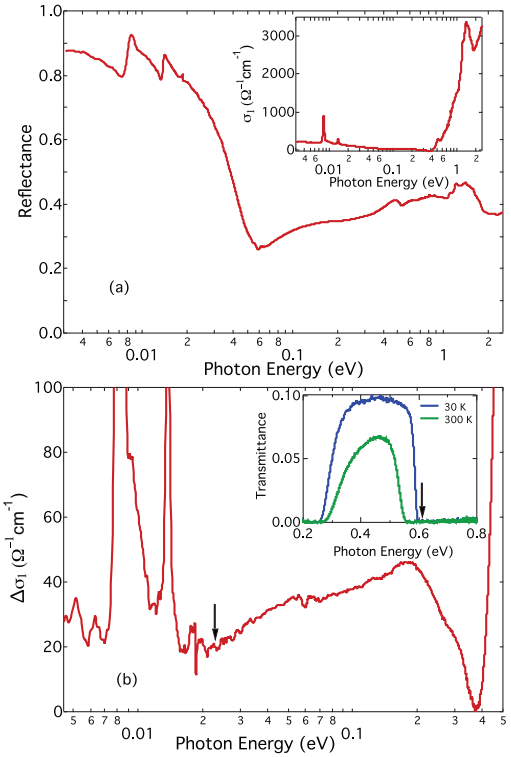

Fig. 4: (Color online) (a) The measured $\mathcal{R}(\omega)$ at $T = 300\,\mathrm{K}$ (main panel) and the optical conductivity $\sigma_1(\omega)$ (inset) of BiTeBr. (b) Main panel: $\Delta\sigma_1(\omega)$ obtained after subtracting the Drude component as explained in the text. The arrow indicates the onset of the first intraband transition. Inset: transmittance of the sample at 30 and 300 K. The arrow indicates E_g, the onset of the bulk interband transitions.

semiconductor. In order to extract the free-carrier properties, we fit both $\mathcal{R}(\omega)$ and $\sigma(\omega)$ with a Drude-Lorentz model [24], optimizing the fit so that the same set of parameters reproduces best both quantities. The fit found a Drude plasma frequency $\omega_p = \sqrt{n_e e^2/m^*\epsilon_0} = 208\,\mathrm{meV}/\hbar$ $(1680\,\mathrm{cm}^{-1})$ and a scattering rate $1/\tau = 25\,\mathrm{meV}/\hbar$ $(200\,\mathrm{cm}^{-1})$. If we assume that the Hall effect originates from bulk carriers and consider the carrier concentration $n_e \approx 5\times10^{18}\,\mathrm{cm}^{-3}$, then the bulk effective mass, obtained from the plasma frequency, is identical to that from SdH oscillations. This agreement further supports the common origin of the carriers responsible both for optical response and for quantum oscillations in BiTeBr.

We now have the information required to calculate the Rashba parameters of BiTeBr, assuming a conduction band configuration and the notation from the upper inset of fig. 1. The energy E_α represents the onset of the intraband transition from the Fermi level of one spin branch to the branch with opposite spin. For small values of the onset, *i.e.*, for the Fermi level close to the crossing point, fig. 1 indicates that $E_\alpha/2$ represents the energy between the Fermi level and the crossing point: $E_\alpha/2 = E_R - E_F$. Assuming parabolic band dispersion $E = \hbar^2k^2/2m^*$, this expression can be written as

$$k_R^2 - k_F^2 = \frac{m^* E_\alpha}{\hbar^2}, \tag{1}$$

where k_R and k_F are the Rashba and the Fermi momenta, respectively, as shown in the upper inset of fig. 1. Next, from the same figure, we can also write

$$k_R + k_F = k_{out}, \tag{2}$$

where $k_{out} = 0.056\,\mathrm{\AA}^{-1}$ is the outer Fermi momentum obtained earlier from the frequency of the SdH oscillations. The optical conductivity gives the energy E_α from the onset of the first (lowest-energy) intraband transition. The main panel of fig. 4(b), shows $\sigma(\omega)$ with the Drude contribution subtracted. The first optical excitation can be clearly identified around $E_\alpha = 24\,\mathrm{meV}$, marked with an arrow in the figure. Above this energy, conductivity, *i.e.*, optical absorption starts increasing monotonically, consistent with an optical transition. Substituting E_α in eq. (1) and solving the system of two equations above, we obtain $k_F = 0.023\,\mathrm{\AA}^{-1}$ and $k_R = 0.033\,\mathrm{\AA}^{-1}$. Then, based on the previous assumption of parabolic band dispersion, the Fermi energy is obtained as $E_F = 14\,\mathrm{meV}$ and the Rashba energy $E_R = 26\,\mathrm{meV}$. Furthermore, we find the bulk coupling strength $\alpha_R = 2E_R/k_R = 1.7\,\mathrm{eV\AA}$. This value, while significantly lower than that determined from ARPES [17], agrees well with theoretical calculations from ref. [16]. We point out here that our result is based on a combination of two robust bulk probes, optical spectroscopy and quantum oscillations, where we ruled out the possible surface origin of the data in both measurements. Moreover, the procedure may serve as a template for determining the bulk electronic properties in Rashba materials, or other semiconductors with strong spin-orbit coupling, such as topological insulators, or bulk Dirac fermions.

In conclusion, we have determined the bulk electronic properties of BiTeBr. We found that BiTeBr is a doped semiconductor, with a band gap $E_g \approx 600\,\mathrm{meV}$. Furthermore, the bulk conduction band shows a Rashba spin splitting with momentum $k_R = 0.033\,\mathrm{\AA}^{-1}$ and energy $E_R = 26\,\mathrm{meV}$. The bulk coupling strength is calculated to be $\alpha_R = 1.7\,\mathrm{eV\AA}$.

* * *

The NHMFL is supported by NSF Cooperative Agreement No. DMR-1157490 and the State of Florida. CM acknowledges support through a grant from the Ramapo College Foundation. We thank Bobby Joe Pullum for support with the experiment at the National High Magnetic Field Laboratory. We also thank Dmitrii Maslov for stimulating discussions.

REFERENCES

[1] Awschalom D. and Samarth N., *Physics*, **2** (2009) 50.
[2] Bihlmayer G., Rader O. and Winkler R., *New J. Phys.*, **17** (2015) 050202 and references therein.

[3] Bychkov Y. A. and Rashba E. I., *J. Phys. C: Solid State Phys.*, **17** (1984) 6039.
[4] Ast C. R., Henk J., Ernst A., Moreschini L., Falub M. C., Pacile D., Bruno P., Kern K. and Grioni M., *Phys. Rev. Lett.*, **98** (2007) 186807.
[5] Mathias S., Ruffing A., Deicke F., Wiesenmayer M., Sakar I., Bihlmayer G., Chulkov E. V., Koroteev Yu. M., Echenique P. M., Bauer M. and Aeschlimann M., *Phys. Rev. Lett.*, **104** (2010) 066802.
[6] Ishizaka K., Bahramy M. S., Murakawa H., Sakano M., Shimojima T., Sonobe T., Koizumi K., Shin S., Miyahara H., Kimura A., Miyamoto K., Okuda T., Namatame H., Taniguchi M., Arita R., Nagaosa N., Kobayashi K., Murakami Y., Kumai R., Kaneko Y., Onose Y. and Tokura Y., *Nat. Mater.*, **10** (2011) 521.
[7] Bahramy M. S., Arita R. and Nagaosa N., *Phys. Rev. B*, **84** (2011) 041202(R).
[8] Landolt G., Eremeev S. V., Koroteev Y. M., Slomski B., Muff S., Kobayashi M., Strocov V. N., Schmitt T., Aliev Z. S., Babanly M. B., Amiraslanov I. R., Chulkov E. V., Osterwalder J. and Dil J. H., *Phys. Rev. Lett.*, **109** (2012) 116403.
[9] Crepaldi A., Moreschini L., Autes G., Tournier-Colletta C., Moser S., Virk N., Berger H., Bugnon Ph., Chang Y. J., Kern K., Bostwick A., Rotenberg E., Yazyev O. V. and Grioni M., *Phys. Rev. Lett.*, **109** (2012) 096803.
[10] Bahramy M. S., Yang B.-J., Arita R. and Nagaosa N., *Nat. Commun.*, **3** (2012) 679.
[11] Xiaoxiang Xi, Chunli Ma, Zhenxian Liu, Zhiqiang Chen, Wei Ku, Berger H., Martin C., Tanner D. B. and Carr G. L., *Phys. Rev. Lett.*, **111** (2013) 155701.
[12] Tran M. K., Levallois J., Lerch P., Teyssier J., Kuzmenko A. B., Auts G., Yazyev O. V., Ubaldini A., Giannini E., van der Marel D. and Akrap A., *Phys. Rev. Lett.*, **112** (2014) 047402.
[13] Chen Y. L., Kanou M., Liu Z. K., Zhang H. J., Sobota J. A., Leuenberger D., Mo S. K., Zhou B., Yang S-L., Kirchmann P. S., Lu D. H., Moore R. G., Hussain Z., Shen Z. X., Qi X. L. and Sasagawa T., *Nat. Phys.*, **9** (2013) 704.
[14] Ying Jian-Jun, Struzhkin Viktor V., Goncharov Alexander F., Mao Ho-Kwang, Chen Fei, Chen Xian-Hui, Gavriliuk Alexander G. and Chen Xiao-Jia, *Phys. Rev. B*, **93** (2016) 100504.
[15] Eremeev S. V., Nechaev I. A., Koroteev Y. M., Echenique P. M. and Chulkov E. V., *Phys. Rev. Lett.*, **108** (2012) 246802.
[16] Eremeev S. V., Rusinov I. P., Nechaev I. A. and Chulkov E. V., *New J. Phys.*, **15** (2013) 075015.
[17] Sakano M., Bahramy M. S., Katayama A., Shimojima T., Murakawa H., Kaneko Y., Malaeb W., Shin S., Ono K., Kumigashira H., Arita R., Nagaosa N., Hwang H. Y., Tokura Y. and Ishizaka K., *Phys. Rev. Lett.*, **110** (2013) 107204.
[18] Jacimovic J., Mettan X., Pisoni A., Gaal R., Katrych S., Demko L., Akrap A., Forro L., Berger H., Bugnon P. and Magrez A., *Scr. Mater.*, **76** (2014) 69.
[19] Tanner D. B., *Phys. Rev. B*, **91** (2015) 035123.
[20] Shoenberg D., *Magnetic Oscillations in Metals* (Cambridge University Press, Cambridge) 1984.
[21] Martin C., Mun E. D., Berger H., Zapf V. S. and Tanner D. B., *Phys. Rev. B*, **87** (2013) 041104(R).
[22] Martin C., Suslov A. V., Buvaev S., Hebard A. F., Bugnon P., Berger H., Magrez A. and Tanner D. B., *Phys. Rev. B*, **90** (2014) 201204(R).
[23] Akrap A., Teyssier J., Magrez A., Bugnon P., Berger H., Kuzmenko A. B. and van der Marel Dirk, *Phys. Rev. B*, **90** (2014) 035201.
[24] Wooten F., *Optical Properties of Solids* (Academic Press, Inc.) 1972.